International Journal of Mass Spectrometry 377 (2015) 179–187

Contents lists available at ScienceDirect

International Journal of Mass Spectrometry

journal homepage: www.elsevier.com/locate/ijms

Gas-phase conformations of small polyprolines and their fragment ions by IRMPD spectroscopy

Jonathan K. Martens [a], Josipa Grzetic [a], Giel Berden [a], Jos Oomens [a,b,*]

[a] Radboud University Nijmegen, Institute for Molecules and Materials, FELIX Facility, Toernooiveld 7, 6525ED Nijmegen, The Netherlands
[b] van't Hoff Institute for Molecular Sciences, University of Amsterdam, Science Park 908, 1098XH Amsterdam, The Netherlands

ARTICLE INFO

Article history:
Received 21 March 2014
Received in revised form 12 July 2014
Accepted 14 July 2014
Available online 18 July 2014

Keywords:
Polyproline
Proline-effect
Peptide fragmentation
Ion spectroscopy
IRMPD
Diketopiperazine-b_2^+

ABSTRACT

Infrared multiple-photon dissociation (IRMPD) spectroscopy has been used to examine the gas-phase conformations of a series of short protonated polyproline ions (Pro_3–Pro_6), their CID/IRMPD fragmentation pathways, and the associated fragment identities. Consistent with previous findings, and in combination with density functional theory (DFT) and MM/MD methods, a series of conformers for the protonated parent ions having their first peptide bond in the *cis* conformation has been identified. This conformation maximizes the solvation of the protonated N-terminus and stabilizes these compact globular-type conformations. This is in contrast to the PPI and PPII polyproline-type helices reported for larger polyproline peptides in solution. As well, this conformation leads to a unique fragmentation pattern upon collisional or multiple-photon activation. We report observation of the uncommon, but thermodynamically favored, diketopiperazine-type b_2^+ fragment ion. Formation of b_2^+ ions along the diketopiperazine pathway is in line with a *cis* configuration of the first amide linkage in the protonated parent ion. Additionally, the parent ion conformations, fragmentation pathways, and proton affinities of the resulting fragments have been related to the observed proline-effect in CID mass spectra.

© 2014 Elsevier B.V. All rights reserved.

1. Introduction

Mass spectrometry has developed into an indispensable tool in modern proteomics and biochemical analysis in general. Complex and sophisticated sequencing algorithms have been developed relating fragmentation patterns to parent ion sequence. However, much of the backbone fragmentation following non-standard pathways remains poorly modeled and the data resulting from these pathways is often not completely utilized [1], possibly resulting in reduced sequence information and less reliable identification. In order to more completely exploit the information contained in protein/peptide MS^n experiments, incorporation of a more comprehensive description of peptide fragmentation mechanisms, including not only models of non-standard fragmentation pathways, but also relative fragment-ion intensity information, is required [2].

The fragmentation of protonated peptides can be described using the mobile proton model, in which a proton normally sequestered at the most basic site in the peptide can localize on amide nitrogen sites following activation [3–7]. This leads to cleavage of the resulting weakened $C(=O)—NH_2^+$ bond and is referred to as the b_n-y_m pathway [8]. As illustrated in Scheme 1 for b_2 formation, this most commonly occurs by nucleophilic attack of the first amide carbonyl oxygen on the carbon of the protonated amide leading to an oxazolone-type fragment [9–11]. Dissociation can also be accomplished with the N-terminal nitrogen acting as the nucleophile, forming a diketopiperazine-type fragment. Within this model, the oxazolone generating reaction requires *trans* conformation of the first peptide bond, while the diketopiperazine analog requires *cis* conformation. The oxazolone-type structure is common and thought to be kinetically favored while the diketopiperazine-type structure is rare, but thermodynamically favored.

While peptide bonds are nearly exclusively in the *trans* configuration, isomerization from *trans* to *cis* conformation of the peptide bond is in some cases thought to be feasible [12–14]. This can be attributed to the weakening and loss of double-bond character of the peptide bond after protonation of the amide nitrogen. This is especially possible when a basic residue traps the proton near to the site of isomerization and has been used to explain the observation of diketopiperazine b-type fragments from protonated histidine-containing peptides [14,15]. In other cases, such as in proline-containing peptides, the peptide bond may exist in the *cis* conformation in advance, making the formation of the

* Corresponding author at: Radboud University, Institute for Molecules and Materials, Toernooiveld 7, 6525ED Nijmegen, The Netherlands.
Tel.: +31 243 653950.
E-mail address: joso@science.ru.nl (J. Oomens).

http://dx.doi.org/10.1016/j.ijms.2014.07.027
1387-3806/© 2014 Elsevier B.V. All rights reserved.

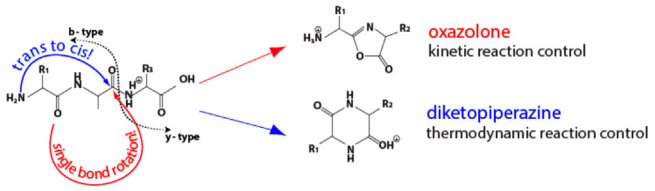

Scheme 1. Different reaction mechanisms for formation of oxazolone and diketopiperazine b-type fragment-ions showing necessary backbone distortions for each reaction.

diketopiperazine b-fragment more easily rationalized. *Cis* peptide bond conformation is commonly cited as occurring in only 0.03–0.05% of cases as a result of both the difference in relative energy of the *cis*/*trans* conformers ($\sim$+10 kJ mol^{-1}) and the high barrier to isomerization ($\sim$85 kJ mol^{-1}) [16,17]. However, for amide bonds involving a proline residue, the *cis*/*trans* conformers are nearly iso-energetic, being separated by only $\sim$2 kJ mol^{-1} and connected by a barrier of approximately 55 kJ mol^{-1} [16,17].

Within the framework of the b_n-y_m fragmentation pathway, the proton is finally shared by the two neutral fragments of the protonated parent in a proton-bound-dimer (PBD) [18]. It is expected that the relative ratio of b_m/y_n ions should qualitatively correspond to the ratios of proton affinities (PAs) between the fragments [8]. As it is generally assumed that the y_n fragment (as a truncated peptide) should have a higher PA than the cyclic diketopiperazine [18], it is expected that upon dissociation of the PBD, the diketopiperazine fragment would often be lost as a neutral and remain unobserved. For oxazolone b-type fragments, having proton affinities typically on the order of the corresponding y-fragments, this is much less the case.

Proline is unique among the common amino acids due to its pyrrolidine ring and the associated rigidity it imparts on the peptide backbone when present. It has been suggested that *cis–trans* isomerization of the peptide bonds in a proline containing-protein is the rate-limiting step in the folding process [19]. Overly-represented fragmentation at Xxx-Pro amide linkages in peptides has been reported in many studies [20–25] and is commonly referred to as the proline effect [26–30]. Additionally, it has been noted that there is an uncommon over-expression of y-type fragment ions in the CID spectra of proline containing-peptides, as well as a dominant b_2^+ ion peak in the case of N-terminal Xxx-Pro occurrences [31]. These effects are often attributed to the high proton affinity of proline and the resulting C-terminal fragments (y-type) as well as the low threshold-energy related to cleavage N-terminal to proline [20]. CID experiments of Pro_8NH_2-H^+ have been used to demonstrate the near absence of b-type ions as well as unbalanced abundances of y-type ions, favoring those resulting from the loss of an even number of proline residues [32]. This fragmentation pattern was found to be dependent on an unblocked N-terminus and the absence of proton sequestering high-basicity residues. Additionally, it was noted that this unique pattern from repeating Pro-residues is not a result of sequential losses of diproline units, but rather the immediate loss of an even number of Pro residues from the protonated parent.

In solution, polyprolines commonly exist as either an all-*cis*, right-handed helix with 3.3 residues per turn (PPI) or an all-*trans* left-handed helix with 3.0 residues per turn (PPII) [33]. These helical structures are unique in that they completely lack hydrogen bonding in their peptide backbones. PPI is stabilized by a tight conformation, maximizing van der Waals interactions, while PPII is stabilized by solvent interactions with the outward facing carbonyl oxygen. PPI is additionally unique in that the macrodipole along the axis of the helix has its partial negative component toward the N-terminus and is thus stabilized by N-terminal protonation. This is in direct contrast to the more common alpha-helix (and others) where the helix is stabilized by an extensive network of backbone hydrogen bonds. In this case, protonation at the N-terminus interacts with the macrodipole in a destabilizing manner as a result of the consistent orientation of the amidic N—H groups toward the N-terminus. Ion mobility experiments and molecular dynamics simulations by Counterman and Clemmer have explored the conformational properties of a large range (over both size and charge state) of polyproline peptides [34]. Small polyprolines were found to mainly adopt conformations that solvate the protonated N-terminus, suggesting that for smaller systems the van der Waals stabilization may be insufficient to promote the formation of the helices. They reported a common structural motif involving *cis* conformation of the first peptide bond in the system, which leads to a bend in the backbone and strong hydrogen bonds between the protonated N-terminus and one or a few of the first carbonyl oxygen. In their simulations, conformations of the remaining amide bonds were found to be of less importance, where possibly a mixture of *cis*/*trans* linkages allowed for more compact gas-phase structures.

Infrared multiple photon dissociation (IRMPD) spectroscopy is a technique that provides direct conformational insight for gas-phase ions and has been applied in the past to identify the conformation of peptide fragment ions [15,35–38]. Here, we use IRMPD spectroscopy in compliment with computational methods to examine the conformations of a series of small polyprolines (3–6 residues) and the influence of the *cis*/*trans* amide bond conformation on their fragmentation pathways.

2. Experimental and computational methods

2.1. Infrared multiple photon dissociation (IRMPD) spectroscopy

Infrared action spectra of protonated peptide and fragment ions were obtained using a previously described Fourier transform-ion cyclotron resonance (FT-ICR) mass spectrometer coupled to the FELIX infrared free electron laser [39]. Protonated molecular ions ($[M+H]^+$) ions were generated using electrospray ionization (ESI) from approximately millimolar peptide solutions in 50:50 acetonitrile:water, acidified with $\sim$0.1% formic acid. Peptide samples were obtained from GeneCust (Luxemburg) at 95% purification and used as received. Pro_2 and Pro_6 were synthesized at Radboud University Nijmegen and cyclo-ProPro was prepared at the University of Amsterdam according to a literature protocol [40]. Following the electrospray process, $[M+H]^+$ ions were accumulated in a linear hexapole trap before being injected into the ICR cell. Peptide fragment ions were generated by nozzle-skimmer dissociation in the high-pressure region at the interface of the electrospray source and the hexapole trap/accumulation region, or directly in the ICR cell by irradiation with a 35 W continuous-wave CO_2 laser for a few hundred milliseconds (ULR-25; Universal Laser Systems, Scottsdale, USA).

Once trapped in the cell, all unwanted ions are ejected by a stored waveform inverse Fourier transform (SWIFT) excitation pulse. The remaining isolated ions are then irradiated by the tunable infrared radiation from FELIX, which arrives as 5 μs macropulses (5 or 10 Hz) of approximately 30–40 mJ with a bandwidth of $\sim$0.4% of the center frequency. Resonant absorption leads to an increase in the internal energy resulting in unimolecular dissociation. This produces a frequency-dependent fragmentation signal which is recorded in the ICR cell using a typical excite/detect procedure. Relation of parent and fragment ion intensities in the observed mass spectral data in terms of the fragmentation yield (ΣI(fragment ions)/ΣI(parent + fragment

ions)) generates the final infrared vibrational action spectrum. The yield at each IR point is obtained from three averaged mass spectra and is linearly corrected for laser power; the frequency is calibrated using a grating spectrometer. IRMPD spectra in the C—H, N—H, and O—H stretching region (2700–3700 cm^{-1}) were obtained using an optical parametric oscillator (OPO, Laser Vision, Bellevue, USA). The Nd:YAG-pumped-OPO generates between 10 and 20 mJ per 5 ns pulse at 10 Hz in the 2700–3700 cm^{-1} range with a bandwidth of approximately 3 cm^{-1}. The IR frequency is calibrated with a wavemeter.

Collision induced dissociation (CID) mass spectral experiments were conducted using a Bruker AmaZon Speed ETD quadrupole ion trap. $[M+H]^+$ ions were generated using electrospray ionization (ESI) from approximately 10 micromolar peptide solutions in 50:50 acetonitrile:water acidified with 0.1% formic acid. After isolation in the trap, the $[M+H]^+$ ions of interest were subjected to CID conditions for 40 ms with amplitude parameters of approximately 0.5–1.0 V.

2.2. Computational chemistry

Even small peptides, such as those considered here, tend to have relatively complex conformational landscapes. As a result, manual definition of input geometries using chemical intuition alone rapidly becomes difficult when considering peptides of sizes larger than 2 and 3 residues. In order to more completely explore the potential energy surface of these peptides, we have therefore employed a molecular mechanics/molecular dynamics (MM/MD) approach using AMBER 12 [41], approximately following a procedure described in more detail previously [42]. Initial guess geometries were first optimized in the Gaussian09 package [43] at the B3LYP/6-31++G(d,p) level of theory. Charges from these initial results were used for parameterization of the nonstandard terminations of the peptides in their predicted non-zwitterionic gas-phase conformations in the antechamber program. After minimization within AMBER, a simulated annealing procedure up to 1000 K was used. With this temperature range it was found that even relatively large barriers, such as *cis*/*trans* isomerization of the peptide bond, were adequately overcome during the simulations of these polyproline peptides. A 1 fs step size was used with coordinates being saved periodically throughout the simulation for individual optimization. The resulting 500 structures were grouped based on structural similarity using appropriate rms criteria (leading to approximately 30 structures for each peptide size). Next, these structures were each optimized at the B3LYP/6-31++G(d,p) level followed by vibrational analysis within the rigid-rotor harmonic oscillator model. Vibrations were scaled by 0.975 in the fingerprint region (800–2000 cm^{-1}), while C—H, N—H, and O—H stretches in the 2700–3700 cm^{-1} region were scaled by 0.955. Calculated stick spectra are broadened using a Gaussian function with a FWHM of 25 cm^{-1} for comparison with experiment. For Pro_3H^+, optimizations on all geometries resulting from the MM/MD procedure were also completed at the B3LYP/6-311+G(d,p) level, and MP2(full)/6-311+G(2d,2p) electronic energies were obtained for optimized geometries at both DFT levels. Finally, harmonic frequencies using the M06 functional as well as anharmonic frequencies at the B3LYP/6-311+G(d,p) level were obtained for the lowest energy conformation of Pro_3H^+. Energies at all three levels of theory were found to be largely consistent. As well, M06 frequencies and anharmonic frequencies were not found to offer improvement over modeling at the B3LYP/6-31++G(d,p) level. These additional calculations are summarized in the supporting information file in Table S1 and Fig. S1. Proton affinities (PAs) and gas-phase basicities (GBs) were calculated using thermodynamic quantities for the protonated and neutral peptides and fragment species at the B3LYP/6-31++G(d,p) level. Specifically, PAs and GBs were calculated as the negative enthalpy change and negative free energy change (at 298.15 K) associated with the relevant protonation reactions, respectively. Numerous proton affinities have been reported for proline [44–48]. While we have here employed only a moderate level of theory, our calculated value of 944 kJ mol^{-1} closely matches the previously reported G3 (MP2) value of 942 kJ mol^{-1} [46]. We use this comparison to justify the, at least qualitative, accuracy of our calculated PAs for the proline-based peptides and fragment ions reported here.

3. Results and discussion

Figs. 1–4 show the IRMPD spectra of Pro_3H^+, Pro_4H^+, Pro_5H^+, and Pro_6H^+ obtained in the 800–1800 cm^{-1} spectral region as well as the 2700–3700 cm^{-1} region of C—H, N—H, and O—H stretches (measurements in the 2700–3700 cm^{-1} region were not obtained for Pro_6H^+). Fig. 5 shows a direct comparison of these experimental spectra. IRMPD spectra of the b_2^+, y_2^+ (from the Pro_3H^+ precursor), and y_3^+ (from the Pro_4H^+ precursor) are presented in Figs. 6, S7 and 1, respectively. CID mass spectra of the protonated parent ions, Pro_2H^+, Pro_3H^+, Pro_4H^+, Pro_5H^+, Pro_6H^+, and Pro_7H^+, are presented in Fig. 7. The MM/MD/DFT procedure described above was used to obtain around 30 optimized geometries and vibrational spectra for each of the Pro_3H^+, Pro_4H^+, Pro_5H^+, Pro_6H^+, and y_2^+ species. The peptide bond dihedral angles, relative electronic energies, enthalpies and Gibbs free energies (298 K) are

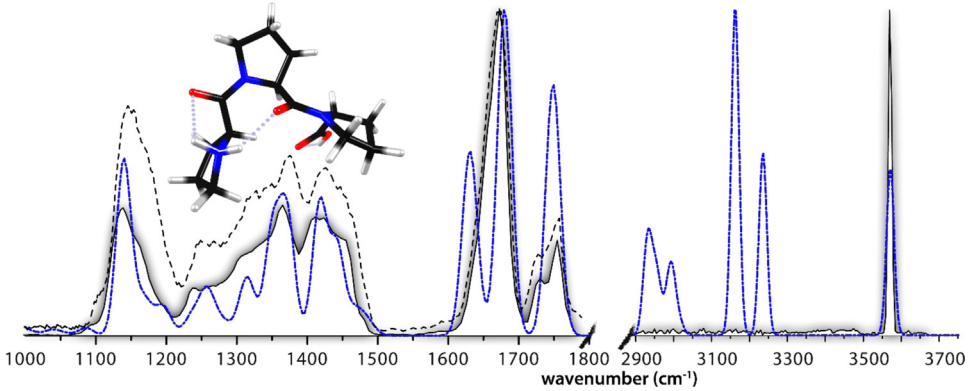

Fig. 1. IRMPD spectrum of Pro_3H^+ shown with the calculated vibrational spectrum of the lowest energy structure, Pro_3H_c1, in blue (structure inlayed) with *cis*/*cis* conformation of the amide bonds in the peptide backbone. The experimental spectrum of the y_3^+ fragment ion produced from CID of Pro_4H^+ is shown in black dashed line.

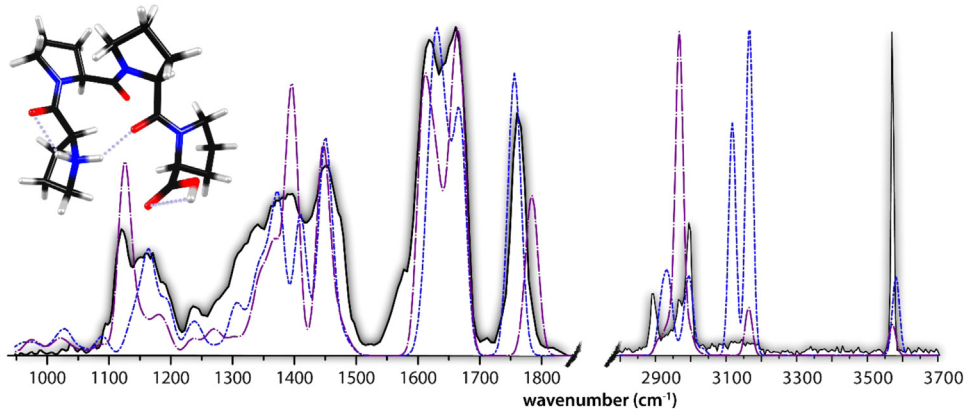

Fig. 2. IRMPD spectrum of Pro_4H^+ shown with the computed vibrational spectrum of the lowest-energy structure (Pro_4H_c3, *cis*/*trans*/*trans*, structure inlayed) in dotted blue and the second lowest energy structure (Pro_4H_c5, 8.7 kJ mol^{-1}, *cis*/*trans*/*cis*) in dashed purple. (For interpretation of the references to color in this figure legend, the reader is referred to the web version of this article.)

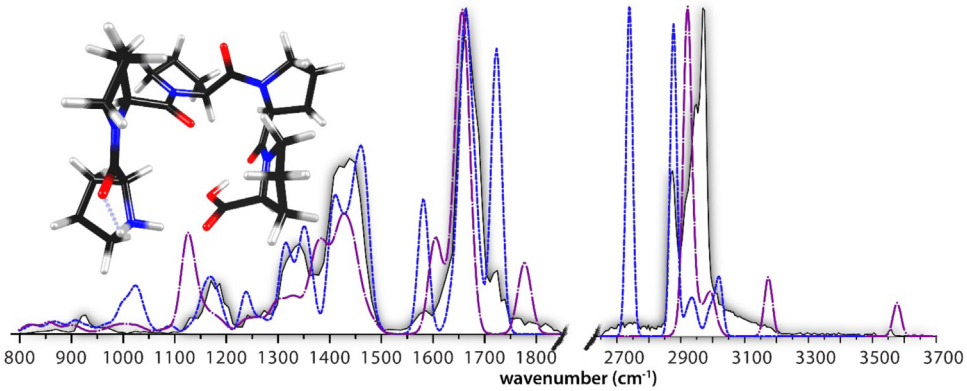

Fig. 3. IRMPD spectrum of Pro_5H^+ shown with calculated vibrational spectrum of the lowest energy calculated structure in dotted blue (Pro_5H_c0, *cis*/*trans*/*cis*/*trans*, structure inlayed) and the second lowest energy calculated structure (Pro_5H_c7, 17.6 kJ mol^{-1}, *cis*/*trans*/*cis*/*trans*) in dashed purple. (For interpretation of the references to color in this figure legend, the reader is referred to the web version of this article.)

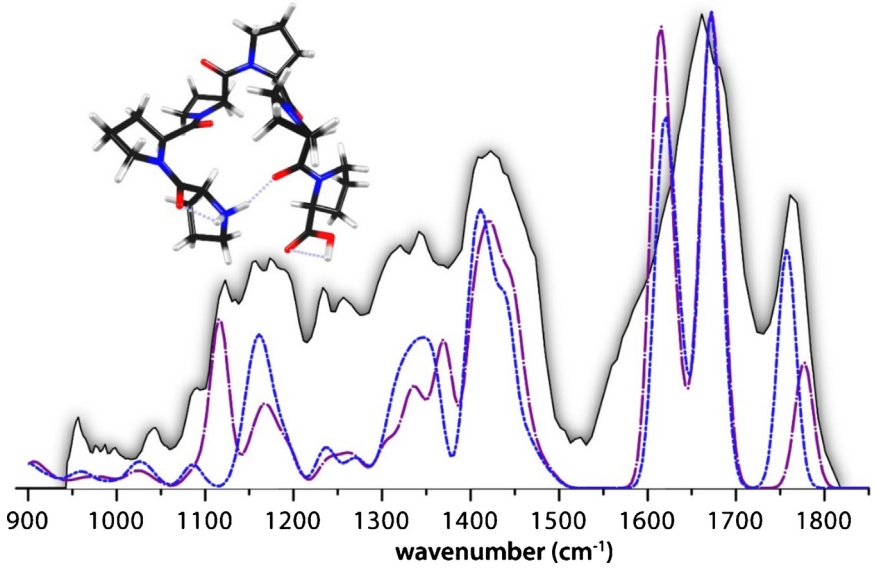

Fig. 4. IRMPD spectrum of Pro_6H^+ shown with the calculated spectra of the lowest energy structure in dotted blue (Pro_6H_c8, *cis*/*trans*/*cis*/*trans*/*trans*, structure inlayed) and the second lowest energy structure (Pro_6H_c15, 2.0 kJ mol^{-1}, *cis*/*trans*/*cis*/*trans*/*trans*) in dashed purple. (For interpretation of the references to color in this figure legend, the reader is referred to the web version of this article.)

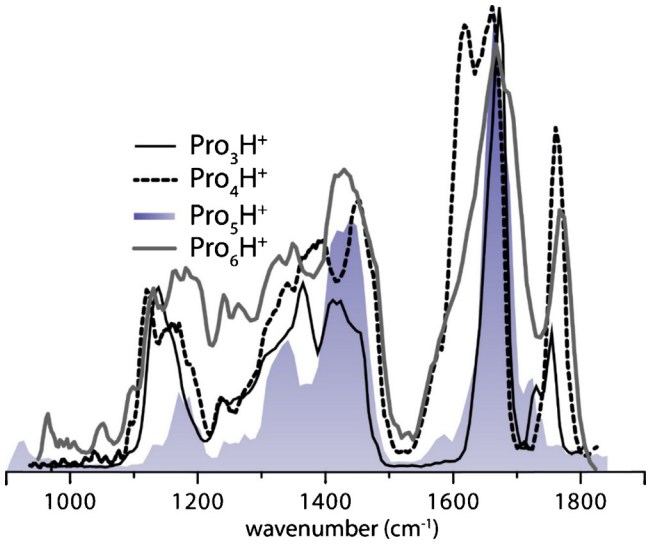

Fig. 5. Overlay of IRMPD spectra for Pro_3H^+, Pro_4H^+, Pro_5H^+ and Pro_6H^+. Pro_5H^+ is markedly different in the 1700–1800 cm^{-1} region due to the alternative conformation of the carboxyl group in comparison with the other oligo-proline peptides.

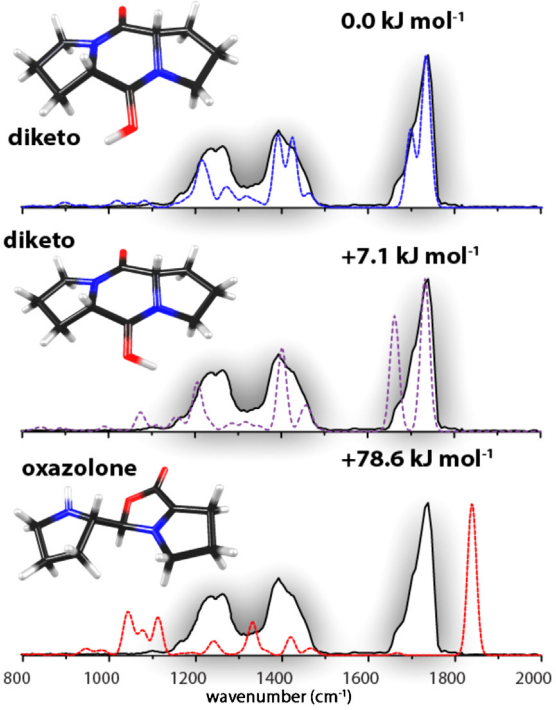

Fig. 6. IRMPD spectrum of the b_2^+ fragment ion from Pro_3H^+ shown with the calculated vibrational spectrum of the lowest-energy diketopiperazine structure in dotted blue and the second lowest diketopiperazine structure in dashed purple. The lowest-energy calculated oxazolone fragment structure is shown in the bottom panel in dashed red line. (For interpretation of the references to color in this figure legend, the reader is referred to the web version of this article.)

presented in Tables S2–S6 for the six lowest energy structures found. Relative free energies and *cis*/*trans* peptide backbone dihedral conformations ($\Omega_{peptide}$, C_α—C(=O)—N—C_α) are listed in captions of Figs. S2–S5 for the low energy structures considered as likely to be contributing to the experimental measurements. Dihedral angles are qualitatively labelled as being in either *cis* or *trans* conformation, however, some variation from zero and 180 degrees does exist in most cases and precise values are given in the supporting information (Tables S2–S6). In the conformational search, different puckering orientations of the proline five-membered ring have been considered, but we have not made any generalizations related to the overall peptide structure [49,50]. Calculated conformations are organized with the addition of an index "_c#" after the name of the peptide.

3.1. Structures of protonated Pro_3, Pro_4, Pro_5, and Pro_6

3.1.1. Structure of Pro_3H^+

The lowest energy calculated conformation of Pro_3H^+, Pro_3H_c1, has both peptide bonds in the *cis* conformation and the protonated N-terminus interacting with both carbonyls of the first and second residues, as well as the C-terminal carboxyl group. The close agreement between the calculated spectrum of this ion and the measured IRMPD spectrum leads us to assign this conformation to that of Pro_3H_c1 under our experimental conditions (see SI for comparison with other low-energy structures). Fig. 1 also contains the IRMPD spectrum of the y_3^+ ion generated from Pro_4H^+. As expected, this spectrum closely matches that of Pro_3H^+ and leads to its assignment as a protonated truncated peptide. The double feature of the carboxyl stretch between 1700 and 1800 cm^{-1} in both the spectrum of Pro_3H^+ and that of the y_3^+ fragment, is unaccounted for by the single band in the calculated structure of Pro_3H_c1 and likely indicates some contribution of a second low-energy conformer, possibly Pro_3H_c3 with a *cis*/*trans* conformation, see Fig. S2. While structure Pro_3H_c3 lies 7.0 kJ mol^{-1} higher and would not be expected to be significant in a Boltzmann population, this energy difference is within the range of computational uncertainty that we infer from relative energy values computed at different levels of theory (Table S1). The calculated spectrum in the 2900–3700 cm^{-1} region contains C—H stretches below 3000 cm^{-1} and N—H stretches between 3100 and 3300 cm^{-1}. These bands are, however, unobserved experimentally because of the relatively low pulse energy from the OPO below ~3000 cm^{-1} and the likely high degree of anharmonicity associated with the strongly hydrogen-bonded amine N—H stretches [51–53]. The unbound carboxyl CO—H stretch at ~3590 cm^{-1} corresponds very well to the experimentally measured band in this region.

3.1.2. Structure of Pro_4H^+

Fig. 2 contains the calculated spectra of the two lowest-energy identified Pro_4H^+ conformers, Pro_4H_c3 and Pro_4H_c5, overlaid on the experimental IRMPD spectrum. While the second lowest-energy conformer, Pro_4H_c5, is calculated to be 8.7 kJ mol^{-1} higher in free energy, the lowest energy conformer, Pro_4H_c3, alone appears to be unable to account for the C—OH bending feature observed around 1100–1200 cm^{-1} and possibly the region of highest intensity immediately to the red of 1400 cm^{-1}. The second lowest energy conformation accounts for these regions nicely and we suspect a mixture of these two conformers to co-exist. The differences in the C—OH bends is likely a result of the long-range weak hydrogen bond involving the C-terminus in Pro_4H_c5 (see Fig. S3) that does not exist in the structure of Pro_4H_c3 shown in Fig. 2.

In the 3 μm spectral range, a small shoulder-peak in the C—H stretching band near 2960 cm^{-1} matches well to the intense peak in the spectrum of the second lowest-energy structure, providing additional support for a fractional presence of this structure. The very weak broadly distributed intensity in the 3100 cm^{-1} region is better accounted for by the lowest-energy conformation, as well as the C—H stretches to the red of 2900 cm^{-1}, although here, the lowest-energy conformation has a small blue-shift in comparison with the experimental band. The free CO—H stretch at ~3590 cm^{-1} is in good agreement with the calculated bands of both structures.

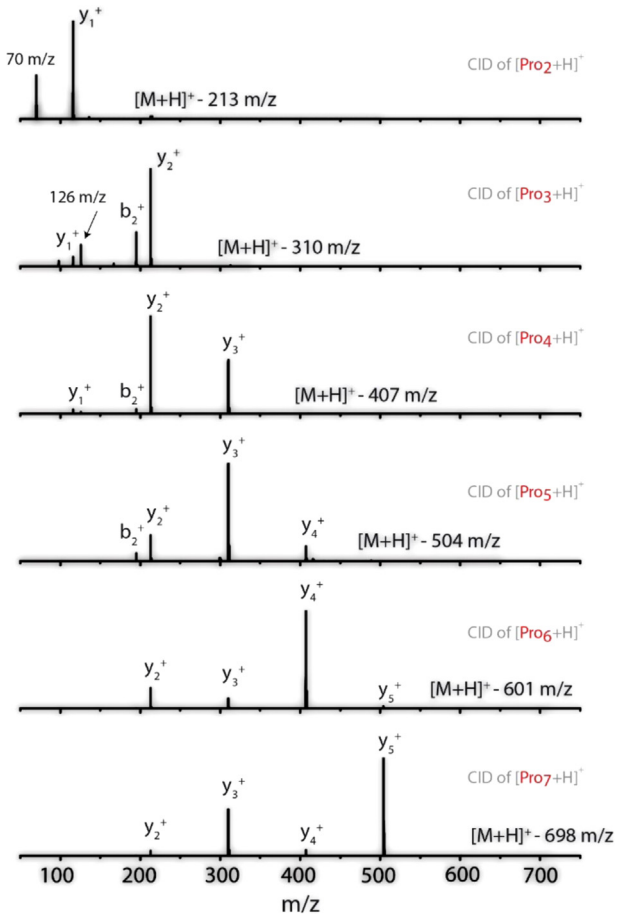

Fig. 7. CID Mass spectra for Pro_nH^+ (n = 2–7) precursor ions. Labelled ions: y_5^+ – 504 m/z, y_4^+ – 407 m/z, b_4^+ – 389, y_3^+ – 310 m/z, y_2^+ – 213 m/z, b_2^+ –195 m/z, 126 m/z (see text for description), y_1^+ – 116 m/z.

3.1.3. Structure of Pro_5H^+

Pro_5H^+ has a somewhat different calculated lowest-energy conformation (Pro_5H_c0) in comparison with Pro_3H^+ and Pro_4H^+, as illustrated in Figs. 3 and S4. The main difference is the conformation of the C-terminal CO—H group, where the proton is shared between the C-terminus and the C=O of the fourth residue. In addition, the N-terminus is interacting with the C=O of the C-terminus and the C=O of the first residue. In this bound conformation, the CO—H stretch is, as expected, red-shifted and broadened and thus unobserved at 3570 cm^{-1}, where it was observed for Pro_3H^+ and Pro_4H^+. There is, however, a very small band observed in the experimental spectrum at 3570 cm^{-1}, attributed to a contribution from a minor population of the second lowest-energy structure (Pro_5H_c7, 17.6 kJ mol^{-1} higher in free energy). The broadly distributed intensity centered at 2700 cm^{-1} corresponds well to the CO—H stretch of the lowest-energy conformation. The C—H stretch bands of the second lowest energy conformation possibly contribute a slight shoulder to the more intense C—H stretching band of the lowest-energy conformation just to the red of 3000 cm^{-1}.

There is relatively clear disagreement between the experimental spectrum and that computed for the second lowest-energy conformer in the fingerprint region, further suggesting the contribution from ions having the second lowest-energy conformation to be very limited. The line positions of the calculated amide I vibrations, carboxyl C=O stretch just above 1700 cm^{-1}, and the N—H scissoring mode at 1580 cm^{-1} for Pro_5H_c0 match nicely with the IRMPD spectrum. Both experimental and calculated spectra above 1550 cm^{-1} are unique from Pro_3H^+ and Pro_4H^+ and clearly contrast the structural differences. The calculated spectrum of Pro_5H_c7, while likely representing a small percentage of the ion population, is again seen to contribute only slightly to the observed spectrum. Possibly, a small shoulder in the experimental COH bend at 1130 cm^{-1} as well as a non-zero baseline around 1775 cm^{-1} is observed from ions having this conformation.

3.1.4. Structure of Pro_6H^+

The IRMPD spectrum of Pro_6H^+, presented in Fig. 4 matches reasonably well with the calculated spectra of the identified low energy structures, Pro_6H_c8 and Pro_6H_c15 (+2.0 kJ mol^{-1}). Other calculated spectra and structures are presented in Fig. S5. The calculated spectrum of Pro_6H_c8, with the N-terminus hydrogen-bonded to the carbonyl group of the fifth residue, matches well in the 1600–1800 cm^{-1} amide I region. Perhaps consideration of the nearly iso-energetic second lowest energy conformation Pro_6H_c15 accounts for the peak near 1125 cm^{-1}. In this conformer, the C-terminus is further away from, and thus less affected by, interaction with the charged N-terminus.

3.1.5. Spectral differences for Pro_3H^+, Pro_4H^+, Pro_5H^+, and Pro_6H^+ related to conformations

The IRMPD spectra of Pro_3H^+ and Pro_4H^+ are fairly similar with only a few distinguishing features, as illustrated in Fig. 5. Indeed, the calculated structures which have been attributed to the experimentally observed spectra are similar. In both structures, the protons of the N-terminus are each hydrogen-bonded to adjacent carbonyl oxygens. In Pro_3H^+, these are the C=O groups of the first and second residues, but for Pro_4H^+ the first and third carbonyl oxygens are bound to the N-terminus, leaving the second amide carbonyl free. As a result, the partly overlapping C=O stretching bands of the three carbonyl groups produce the double-featured appearance of the amide I peak. The NH_2-scissoring mode of the protonated N-terminus is overlapping with this peak.

In the calculated spectrum of Pro_3H^+, the carbonyl stretch of the first residue is observed at approximately at 1680 cm^{-1}, while two overlapping modes at approximately 1630 cm^{-1} are both coupled motions of the second carbonyl stretching and the protonated N-terminus scissoring.

In contrast to Pro_3H^+ and Pro_4H^+, the amide I band for Pro_5H^+ is nearly overlapping with the red-shifted carboxyl C=O stretch, likely as a result of the different bonding environment of the C-terminus. The Pro_4H^+ COH bending peak just to the blue of 1100 cm^{-1} has a double feature in the IRMPD spectrum likely due to the contribution of the second lowest energy structure (illustrated in Fig. 2). This is not observed for Pro_3H^+. Pro_5H^+ does not have a peak in this region, as expected, due to hydrogen-bonding of the CO—H with the carbonyl oxygen of the fourth residue. The peak just below 1200 cm^{-1} in the spectrum of Pro_5H^+ is mainly from coupled —CH_2— ring vibrations, likely corresponding to the small shoulder of the C—OH bending peak for Pro_4H^+, and possibly Pro_3H^+.

The spectrum of Pro_6H^+ is again similar those observed for Pro_3H^+ and Pro_4H^+, suggesting a general structural pattern for polyprolines, with Pro_5H^+ as somewhat of an exception in the series. Generally speaking, the IRMPD spectra of these four protonated peptides exhibit similar overall features, while the details nicely distinguish the structural differences in the conformations.

In general, the *cis* versus *trans* configuration of the first peptide bond is seen to have a distinct effect on the overall conformation of the peptide. For example, for Pro_3H^+ in Fig. S2, the three mostly extended structures (c4, c6, and c2) all have a *trans* configuration of the first peptide bond. This results in a different bonding environment for the N-terminus, the central C=O moiety and

Table 1
CID fragments formed from $Pro_{2-7}H^+$ (%).

	Pro_2H^+	Pro_3H^+	Pro_4H^+	Pro_5H^+	Pro_6H^+	Pro_7H^+
m/z 70	29.0	–	–	–	–	–
y_1^+	71.0	5.5	2.6	–	–	–
m/z 126	–	11.9	1.4	–	–	–
a_2^+	–	1.8	0.3	0.4	–	–
b_2^+	–	21.0	3.3	5.5	0.2	0.4
y_2^+	–	59.7	58.8	16.6	14.1	3.1
y_3^+	–	–	33.7	67.1	7.3	27.3
y_4^+	–	–	–	10.5	76.3	3.8
y_5^+	–	–	–	–	2.0	65.3
Σy_n^+/total frag. int.	71.0	65.2	95.1	94.2	99.8	99.6

the C-terminus, in comparison to the structures with a *cis* conformation of the first peptide bond and more compact structures (c1, c3, and c0). Considering Figs. S2 (structures c4, c6, and c2), S4 (structure c2) and S5 (structure c31), one can see that in all cases where the first peptide bond is *trans,* a more elongated structure results, where the N-terminus tends to be less solvated. As the N-terminus is one of only two possible hydrogen bond donors in these peptides, this is likely related to the increased stability of the more compact conformations resulting from a *cis* configured first peptide linkage.

3.2. Fragments and dissociation pathways of Pro_3H^+

3.2.1. Structure of Pro_3H^+ b_2^+

IR spectroscopy of the b_2^+ fragment generated from Pro_3H^+ clearly shows that this fragment ion is of diketopiperazine type (see Fig. 6). This can be inferred from the close spectral match with the spectrum calculated for the lowest-energy structure, which is of diketopiperazine type, and with the experimental IRMPD spectrum generated from the synthetic protonated cyclo-ProPro (see Fig. S6). Additionally, the b_2^+ experimental spectrum shows no sign of a band near 1850 cm^{-1}, where the oxazolone C=O stretch would typically be found [35]; the calculated diketopiperazine amide C=O stretch at 1730 cm^{-1} matches favorably with experiment. Comparison with other calculated diketopiperazine structures, protonated at different sites and with different ring conformations (not shown), confirmed the assignment of the oxygen-protonated structure shown here. A shoulder in the experimental band to the red of 1700 cm^{-1} suggests that a portion of the sampled ions exists as the calculated higher-energy rotamer of the lowest-energy structure shown in the middle panel of Fig. 6. Although only separated by 7.1 kJ mol^{-1} (see Table S7), interconversion between these two structures was computed to have a barrier of approximately 35 kJ mol^{-1}.

3.2.2. Structure of the y_2^+ fragment of Pro_3H^+

Fig. S7 contains the IRMPD spectrum of the y_2^+ fragment ion derived from Pro_3H^+ as well as the calculated spectra for the lowest and, nearly-degenerate, second lowest-energy structures of the truncated peptide Pro_2H^+. Interestingly, these two conformations differ only by the *cis/trans* orientation of the peptide bond, with the *trans* conformation being 1.8 kJ mol^{-1} lower in free energy. This change in peptide bond conformation results in the first carbonyl group interacting with the other proton of the protonated N-terminus, and being closer to the —CH_2— group of the proline ring instead of the proton attached to the α-carbon of the second residue. Such minor structural differences, predictably, result in very similar vibrational spectra, with the main differences being in the experimentally unobserved C—H stretches below 3000 cm^{-1} and the 1200–1300 cm^{-1} region of the fingerprint spectra. While the experimental spectrum matches qualitatively better to the lowest-energy *trans* conformation (blue), the contrast with the calculated spectrum of the second lowest-energy conformation is insufficient to assign one structure to the experimentally measured ion population. Additionally, consideration of the calculated free energies would suggest a mixture of these two conformations at room temperature.

3.2.3. CID of $Pro_{2-7}H^+$

Structural insight from the IRMPD results discussed above, as well as calculated thermochemical properties obtained for the matching conformations, provides valuable information for interpreting the observed CID fragmentation patterns of these polyprolines. Table 1 contains a list of the significant fragments observed after CID of the protonated Pro_2H^+—Pro_7H^+ parent ions presented in Fig. 7. For Pro_nH^+ (n = 4–7) the most intense fragments are the y_{n-2}^+ ions [32] and very little intensity was observed for any of the b_m^+ ions and for the y_1^+ fragment. Pro_3H^+ is markedly different in its fragmentation pattern, having an intense b_2^+ signal. Pro_3H^+ has been previously reported to form mainly y- and b-type fragments (67.6% – y_2^+, 29.7% – b_2^+) and additionally at higher energies an ion at *m/z* 126 [22]. This ion was proposed to be formed from both the b_2^+ ion and the $[M+H]^+$ precursor. These results are in close agreement with the presently reported CID results, with only small amounts of the a_2^+ and y_1^+ ions being observed here in addition.

Fragmentation along the b_m-y_n pathway reportedly results in a proton-bound-dimer of the complementary neutral fragments [4]. Upon dissociation of the dimer, the fragment retaining the proton will be the one observed in the mass spectrum and its counterpart will be lost as a neutral. Presumably, the fragment with the higher PA is expected to predominantly retain the proton. Table 2 lists the PAs and GBs of Pro_3 and its observed fragments. As y_n-type fragments are thought to correspond to truncated peptides (see also Fig. S6), the calculated peptide PAs are also taken as the PAs of the corresponding neutral y_n-type fragments. As illustrated in Table 2, the PA of the diketopiperazine b-type fragment is lower than both the oxazolone b-fragment and any of the y_n fragments considered (themselves comparable). This is consistent with the near absence of b-ions in the fragmentation patterns observed for Pro_4H^+, Pro_5H^+, Pro_6H^+, and Pro_7H^+ assuming that the b_2 fragments have diketopiperazine and not oxazolone structure. This assumption appears justified by the fact that all of the low-energy conformations for Pro_3H^+, Pro_4H^+, Pro_5H^+, and Pro_6H^+ identified here from the IRMPD spectra have *cis* conformation of their first

Table 2
Proton affinities and gas-phase basicities of Pro_3 and associated fragment ions (kJ mol^{-1}).

B3LYP/6-31++G(d,p)	PA	GB	Fragment label
Pro_3	1028	1003	y_3^+
Pro_2	996	972	y_2^+
Proline	944	922	y_1^+
b_2-oxazolone	1025	1009	b_2^+
b_2-diketo	888	868	b_2^+

peptide bond. The values in Table 2, however, do not explain the observed intensity ratios of the b_2^+ and y_1^+ fragments for Pro_3H^+, although for this combination, the PA-difference between b_2 and y_{n-2} fragments is by far the smallest in the series considered. Clearly the fragmentation patterns observed here cannot be simply described using thermodynamic arguments and considerations of the internal energy distribution of the ions as well as kinetic factors need to be considered.

4. Conclusions

In summary, the results presented here indicate that the b_2 fragment of Pro_3H^+ is characteristic of the thermodynamically-favored diketopiperazine structure, showing no band higher than 1800 cm^{-1}, where an oxazolone carbonyl stretch would typically be found. This leads us to assign this ion to be one of only a few cases where a b-type fragment does not form on the so-called oxazolone pathway. Additionally, we observed collisional activation of the larger polyprolines to produce mainly y-type fragments. Computations show that *y*-ions of increasing size are increasingly likely to retain the proton in the dissociation process, particularly when the complementary N-terminal b_2-fragment possesses a diketopiperazine structure. This is due to the substantially lower proton affinity of the diketopiperazine structure as compared to the oxazolone b_2-structure.

Further evidence for the formation of diketopiperazine b_2-fragments is provided by IR spectroscopy, establishing that the first peptide bond in the protonated polyproline precursor ions is generally in the *cis*-configuration. The IRMPD spectrum of protonated Pro_3 matches nicely with the calculated spectrum of the lowest energy conformation identified here, having both amide bonds in the *cis* configuration. For Pro_4H^+, Pro_5H^+, and Pro_6H^+, the experimental spectra match with calculated structures having mixed *cis* and *trans* peptide bonds, however, the first amide bond was found to be *cis* in all cases. In these conformations, the protonated N-terminus can hydrogen-bond with the carbonyl oxygens; recall that apart from the terminal ends of the peptide, there exist no H-bond donors in polyproline peptides. Hence, establishing that the first peptide bond is generally in a *cis*-configuration supports the proposition of a diketopiperazine-b_2 fragment for protonated polyprolines.

Acknowledgments

The authors gratefully acknowledge Mr. S. Popovic and Dr. J. van Maarseveen from the University of Amsterdam for synthesizing the cyclo-ProPro model compound as well as Dr. D. Löwik from the Radboud University for synthesizing the Pro_2 and Pro_6 peptides. They gratefully acknowledge the FELIX staff, particularly Dr. A.F.G. van der Meer, Dr. B. Redlich and Mr. R. van Buuren for technical support. Financial support for this project was provided by NWO Chemical Sciences under VICI project no. 724.011.002. The authors also thank NWO Physical Sciences (EW) and the SARA Supercomputer Center for providing the computational resources (grants MP-264-14 and SH-260-14). This work is part of the research program of FOM, which is financially supported by NWO.

Appendix A. Supplementary data

Supplementary data associated with this article can be found, in the online version, at http://dx.doi.org/10.1016/j.ijms.2014.07.027.

References

[1] Y. Huang, G.C. Tseng, S. Yuan, L. Pasa-Tolic, M.S. Lipton, R.D. Smith, V.H. Wysocki, A data-mining scheme for identifying peptide structural motifs responsible for different MS/MS fragmentation intensity patterns, J. Proteome Res. 7 (1) (2007) 70–79.
[2] W. Li, L. Ji, J. Goya, G. Tan, V.H. Wysocki, An intensity-incorporated protein identification algorithm for tandem mass spectrometry, J. Proteome Res. 10 (4) (2011) 1593–1602.
[3] V.H. Wysocki, G. Tsaprailis, L.L. Smith, L.A. Breci, Mobile and localized protons: a framework for understanding peptide dissociation, J. Mass Spectrom. 35 (12) (2000) 1399–1406.
[4] B. Paizs, S. Suhai, Fragmentation pathways of protonated peptides, Mass Spectrom. Rev. 24 (4) (2005) 508–548.
[5] K.A. Cox, S.J. Gaskell, M. Morris, A. Whiting, Role of the site of protonation in the low-energy decompositions of gas-phase peptide ions, J. Am. Soc. Mass Spectrom. 7 (6) (1996) 522–531.
[6] R. Boyd, Somogyi Á, The mobile proton hypothesis in fragmentation of protonated peptides: a perspective, J. Am. Soc. for Mass Spectrom. 21 (8) (2010) 1275–1278.
[7] A.R. Dongré, J.L. Jones, Á Somogyi, V.H. Wysocki, Influence of peptide composition, gas-phase basicity, and chemical modification on fragmentation efficiency: evidence for the mobile proton model, J. Am. Chem. Soc. 118 (35) (1996) 8365–8374.
[8] B. Paizs, S. Suhai, Towards understanding the tandem mass spectra of protonated oligopeptides. 1: mechanism of amide bond cleavage, J. Am. Soc. Mass Spectrom. 15 (1) (2004) 103–113.
[9] T. Yalcin, C. Khouw, I.G. Csizmadia, M.R. Peterson, A.G. Harrison, Why are B ions stable species in peptide spectra? J. Am. Soc. Mass Spectrom. 6 (12) (1995) 1165–1174.
[10] T. Yalcin, I.G. Csizmadia, M.R. Peterson, A.G. Harrison, The structure and fragmentation of Bn ($n \geq 3$) ions in peptide spectra, J. Am. Soc. Mass Spectrom. 7 (3) (1996) 233–242.
[11] A.G. Harrison, I.G. Csizmadia, T.-H. Tang, Structure and fragmentation of b_2 ions in peptide mass spectra, J. Am. Soc. Mass Spectrom. 11 (5) (2000) 427–436.
[12] B. Paizs, S. Suhai, Combined quantum chemical and RRKM modeling of the main fragmentation pathways of protonated GGG. I. *Cis–trans* isomerization around protonated amide bonds, Rapid Commun. Mass Spectrom. 15 (23) (2001) 2307–2323.
[13] B. Paizs, S. Suhai, Combined quantum chemical and RRKM modeling of the main fragmentation pathways of protonated GGG. II. Formation of b_2, y_1, and y_2 ions, Rapid Commun. Mass Spectrom. 16 (5) (2002) 375–389.
[14] A.C. Gucinski, J. Chamot-Rooke, E. Nicol, Á Somogyi, V.H. Wysocki, Structural influences on preferential oxazolone versus diketopiperazine b_2^+ ion formation for histidine analogue-containing peptides, J. Phys. Chem. A 116 (17) (2012) 4296–4304.
[15] B.R. Perkins, J. Chamot-Rooke, S.H. Yoon, A.C. Gucinski, Á Somogyi, V.H. Wysocki, Evidence of diketopiperazine and oxazolone structures for HA b_2^+ ion, J. Am. Chem. Soc. 131 (48) (2009) 17528–17529.
[16] D. Pal, P. Chakrabarti, *Cis* peptide bonds in proteins: residues involved, their conformations, interactions and locations, J. Mol. Biol. 294 (1) (1999) 271–288.
[17] A. Jabs, M.S. Weiss, R. Hilgenfeld, Non-proline *cis* peptide bonds in proteins, J. Mol. Biol. 286 (1) (1999) 291–304.
[18] M.J. Nold, B.A. Cerda, C. Wesdemiotis, Proton affinities of the N- and C-terminal segments arising upon the dissociation of the amide bond in protonated peptides, J. Am. Soc. Mass Spectrom. 10 (1) (1999) 1–8.
[19] J.F. Brandts, M. Brennan, L.-N. Lin, Unfolding and refolding occur much faster for a proline-free proteins than for most proline-containing proteins, Proc. Natl. Acad. Sci. 74 (10) (1977) 4178–4181.
[20] C. Bleiholder, S. Suhai, A. Harrison, B. Paizs, Towards understanding the tandem mass spectra of protonated oligopeptides. 2: the proline effect in collision-induced dissociation of protonated Ala-Ala-Xxx-Pro-Ala (Xxx = Ala-Ser-Leu-Val-Phe and Trp), J. Am. Soc. Mass Spectrom. 22 (6) (2011) 1032–1039.
[21] L.A. Breci, D.L. Tabb, J.R. Yates, V.H. Wysocki, Cleavage N-terminal to proline; analysis of a database of peptide tandem mass spectra, Anal. Chem. 75 (9) (2003) 1963–1971.
[22] R.N. Grewal, H. El Aribi, A.G. Harrison, K.W.M. Siu, A.C. Hopkinson, Fragmentation of protonated tripeptides: the proline effect revisited, J. Phys. Chem. B 108 (15) (2004) 4899–4908.
[23] A.G. Harrison, A.B. Young, Fragmentation reactions of deprotonated peptides containing proline. The proline effect, J. Mass Spectrom. 40 (9) (2005) 1173–1186.
[24] B.L. Schwartz, M.M. Bursey, Some proline substituent effects in the tandem mass spectrum of protonated pentaalanine, Biol. Mass Spectrom. 21 (2) (1992) 92–96.
[25] T. Vaisar, J. Urban, Probing proline effect in CID of protonated peptides, J. Mass Spectrom. 31 (10) (1996) 1185–1187.
[26] J.A. Loo, C.G. Edmonds, R.D. Smith, Tandem mass spectrometry of very large molecules. 2. Dissociation of multiply charged proline-containing proteins from electrospray ionization, Anal. Chem. 65 (4) (1993) 425–438.
[27] D.F. Hunt, J.R. Yates, J. Shabanowitz, S. Winston, C.R. Hauer, Protein sequencing by tandem mass spectrometry, Proc. Natl. Acad. Sci. 83 (17) (1986) 6233–6237.
[28] S.A. Martin, K. Biemann, A comparison of keV atom bombardment mass spectra of peptides obtained with a two-sector mass spectrometer with those from a four-sector tandem mass spectrometer, Int. J. Mass Spectrom. Ion Process. 78 (0) (1987) 213–228.
[29] X.J. Tang, P. Thibault, R.K. Boyd, Fragmentation reactions of multiply-protonated peptides and implications for sequencing by tandem mass spectrometry with low-energy collision-induced dissociation, Anal. Chem. 65 (20) (1993) 2824–2834.

[30] T. Vaisar, J. Urban, Gas-phase fragmentation of protonated mono-*N*–methylated peptides. Analogy with solution-phase acid-catalyzed hydrolysis, J. Mass Spectrom. 33 (6) (1998) 505–524.
[31] E.A. Kapp, F. Schütz, G.E. Reid, J.S. Eddes, R.L. Moritz, R.A.J. O'Hair, T.P. Speed, R.J. Simpson, Mining a tandem mass spectrometry database to determine the trends and global factors influencing peptide fragmentation, Anal. Chem. 75 (22) (2003) 6251–6264.
[32] A.G. Unnithan, M.J. Myer, C.J. Veale, A.S. Danell, MS/MS of protonated polyproline peptides: the influence of N-terminal protonation on dissociation, J. Am. Soc. Mass Spectrom. 18 (12) (2007) 2198–2203.
[33] M. Moradi, V. Babin, C. Roland, T.A. Darden, C. Sagui, Conformations and free energy landscapes of polyproline peptides, Proc. Natl. Acad. Sci. 106 (49) (2009) 20746–20751.
[34] A.E. Counterman, D.E. Clemmer, Anhydrous polyproline helices and globules, J. Phys. Chem. B 108 (15) (2004) 4885–4898.
[35] J. Oomens, S. Young, S. Molesworth, M. Stipdonk, Spectroscopic evidence for an oxazolone structure of the b_2 fragment ion from protonated tri-alanine, J. Am. Soc. for Mass Spectrom. 20 (2) (2009) 334–339.
[36] S. Durand, M. Rossa, O. Hernandez, B. Paizs, P. Maître, IR spectroscopy of b4 fragment ions of protonated pentapeptides in the XH (XC,N, O) region, J. Phys. Chem. A 117 (12) (2013) 2508–2516.
[37] S.H. Yoon, J. Chamot-Rooke, B.R. Perkins, A.E. Hilderbrand, J.C. Poutsma, V.H. Wysocki, IRMPD spectroscopy shows that AGG forms an oxazolone b_2^+ ion, J. Am. Chem. Soc. 130 (52) (2008) 17644–17645.
[38] J. Grzetic, J. Oomens, Spectroscopic identification of cyclic imide b_2-ions from peptides containing Gln and Asn residues, J. Am. Soc. Mass Spectrom. 24 (8) (2013) 1228–1241.
[39] J.J. Valle, J.R. Eyler, J. Oomens, D.T. Moore, A.F.G. van der Meer, G. von Helden, G. Meijer, C.L. Hendrickson, A.G. Marshall, G.T. Blakney, Free electron laser-Fourier transform ion cyclotron resonance mass spectrometry facility for obtaining infrared multiphoton dissociation spectra of gaseous ions, Rev. Sci. Instrum. 76 (2) (2005) 23103.
[40] A. Friedrich, M. Jainta, M. Nieger, S. Bräse, One-Pot synthesis of symmetrical and unsymmetrical diketopiperazines from unprotected amino acids, Synlett. 2007, (2007) 2127–2129 (EFirst).
[41] D.A. Case TAD, T.E. Cheatham III, C.L. Simmerling, J. Wang, R.E. Duke, R. Luo, R.C. Walker, W. Zhang, K.M. Merz, B. Roberts, S. Hayik, A. Roitberg, G. Seabra, J. Swails, A.W. Goetz, I. Kolossváry, K.F. Wong, F. Paesani, J. Vanicek, R.M. Wolf, J. Liu, X. Wu, S.R. Brozell, T. Steinbrecher, H. Gohlke, Q.X. Cai Ye, J. Wang, M.-J. Hsieh, G. Cui, D.R. Roe, D.H. Mathews, M.G. Seetin, R. Salomon-Ferrer, C. Sagui, V. Babin, T. Luchko, S. Gusarov, A. Kovalenko, P.A. Kollman, AMBER, University of California, San Francisco, 2012.
[42] C.N. Stedwell, J.F. Galindo, K. Gulyuz, A.E. Roitberg, N.C. Polfer, Crown complexation of protonated amino acids: influence on IRMPD spectra, J. Phys. Chem. A 117 (6) (2012) 1181–1188.
[43] M.J. Frisch, G.W. Trucks, H.B. Schlegel, G.E. Scuseria, A. RobbM, J.R. Cheeseman, G. Scalmani, V. Barone, B. Mennucci, G.A. Petersson, H. Nakatsuji, M. Caricato, X. Li, H.P. Hratchian, A.F. Izmaylov, J. Bloino, G. Zheng, J.L. Sonnenberg, M. Hada, M. Ehara, K. Toyota, R. Fukuda, J. Hasegawa, M. Ishida, T. Nakajima, Y. Honda, O. Kitao, H. Nakai, T. Vreven, J.A. Montgomery, J.E. Peralta, F. Ogliaro, M. Bearpark, J.J. Heyd, E. Brothers, K.N. Kudin, V.N. Staroverov, R. Kobayashi, J. Normand, K. Raghavachari, A. Rendell, J.C. Burant, S.S. Iyengar, J. Tomasi, M. Cossi, N. Rega, J.M. Millam, M. Klene, J.E. Knox, J.B. Cross, V. Bakken, C. Adamo, J. Jaramillo, R. Gomperts, R.E. Stratmann, O. Yazyev, A.J. Austin, R. Cammi, C. Pomelli, J.W. Ochterski, R.L. Martin, K. Morokuma, V.G. Zakrzewski, G.A. Voth, P. Salvador, J.J. Dannenberg, S. Dapprich, A.D. Daniels, Farkas, J.B. Foresman, J.V. Ortiz, J. Cioslowski, D.J. Fox, Gaussian 09, Revision D .01, Wallingford CT, 2009.
[44] C. Bleiholder, S. Suhai, B. Paizs, Revising the proton affinity scale of the naturally occurring α-amino acids, J. Am. Soc. Mass Spectrom. 17 (9) (2006) 1275–1281.
[45] A.G. Harrison, The gas-phase basicities and proton affinities of amino acids and peptides, Mass Spectrom. Rev. 16 (4) (1997) 201–217.
[46] S. Gronert, D.C. Simpson, K.M. Conner, A reevaluation of computed proton affinities for the common α-amino acids, J. Am. Soc. Mass Spectrom. 20 (11) (2009) 2116–2123.
[47] T.C. Dinadayalane, G.N. Sastry, J. Leszczynski, Comprehensive theoretical study towards the accurate proton affinity values of naturally occurring amino acids, Int. J. Quantum Chem. 106 (14) (2006) 2920–2933.
[48] E.P.L. Hunter, S.G. Lias, Evaluated gas phase basicities and proton affinities of molecules: an update, J. Phys. Chem. Ref. Data 27 (3) (1998) 413–656.
[49] T. Marino, N. Russo, M. Toscano, Interaction of Li^+, Na^+, and K^+ with the proline amino acid. Complexation modes, potential energy profiles, and metal ion affinities, J. Phys. Chem. B 107 (11) (2003) 2588–2594.
[50] E.J. Milner-White, L.H. Bell, P.H. Maccallum, Pyrrolidine ring puckering in *cis* and *trans*-proline residues in proteins and polypeptides: different puckers are favoured in certain situations, J. Mol. Biol. 228 (3) (1992) 725–734.
[51] A. Sediki, L.C. Snoek, M.-P. Gaigeot, NH^+ vibrational anharmonicities directly revealed from DFT-based molecular dynamics simulations on the Ala_7H^+ protonated peptide, Int. J. Mass Spectrom. 308 (2–3) (2011) 281–288.
[52] A. Cimas, T.D. Vaden, T.S.J.A. de Boer, L.C. Snoek, M.P. Gaigeot, Vibrational spectra of small protonated peptides from finite temperature MD simulations and IRMPD spectroscopy, J. Chem. Theory Comput. 5 (4) (2009) 1068–1078.
[53] C.M. Leavitt, A.F. DeBlase, C.J. Johnson, M. van Stipdonk, A.B. McCoy, M.A. Johnson, Hiding in plain sight: unmasking the diffuse spectral signatures of the protonated N-terminus in isolated dipeptides cooled in a cryogenic ion trap, J. Phys. Chem. Lett. 4 (20) (2013) 3450–3457.